Post-mortem examination combined with one-time chemical cleaning of fouled flat sheet PVDF-based membrane element used in MBR for TiO$_2$ particle separation

Kayode Hassan Lasisi[a,b,c], Fang Fang[a], Kaisong Zhang[a,*], Temitope Fausat Ajibade[a,b,c], Weihao Yao[a,b], Qiang Xue[a,b]

[a]Key Laboratory of Urban Pollutant Conversion, Institute of Urban Environment, Chinese Academy of Sciences, Xiamen 361021, China, emails: kszhang@iue.ac.cn (K. Zhang), lasisi@iue.ac.cn (K.H. Lasisi), ffang@iue.ac.cn (F. Fang), temitope@iue.ac.cn (T.F. Ajibade), whyao@iue.ac.cn (W. Yao), qxue@iue.ac.cn (Q. Xue)
[b]University of Chinese Academy of Sciences, Beijing 100049, China
[c]Department of Civil and Environmental Engineering, Federal University of Technology Akure, PMB 704, Nigeria

ABSTRACT

A detailed post-mortem study of fouling formation mechanism and cleaning behavior of fouled membrane elements, used for titanium dioxide (TiO$_2$) particle separation is of great significance. In this study, a simple but systematic membrane post-mortem analytical procedure was used to investigate foulant composition, fouling formation mechanism and one-time cleaning behavior of fouled flat sheet polyvinylidene fluoride-based membrane elements, used in membrane bioreactor for separating TiO$_2$ particle. This was achieved by attenuated total reflectance–Fourier-transform infrared spectroscopy, X-ray diffraction, scanning electron microscopy, energy-dispersive X-ray spectrometer, zeta-potential, contact angle, visual inspection, pure water flux, cleaning efficiency and porosity analysis. The morphology, elemental composition and structural result analysis show the scaling elements such as S, Fe, Si, Ti and Al as primary contributors to the overall fouling of the membrane. The zeta potential, contact angle and porosity analysis revealed the electrostatic interactions and adhesion mechanism between the foulant and the membrane surface which were negatively charged and hydrophilic in nature. The chemical cleaning result reveals that 3 M NaClO gave the best cleaning efficiencies having pure water flux of 1,212.7 ± 70.79 and 783.62 ± 26.14 L m^{-2} h^{-1} and flux recovery of 81% and 51% for cross-flow and dead-end filtration units respectively while the use of H$_2$O$_2$ at higher concentration shows tendencies of refouling the membrane surface.

Keywords: Membrane post-mortem; Polyvinylidene fluoride; Membrane fouling; Chemical cleaning; Membrane bioreactor; Titanium dioxide

1. Introduction

In recent decades, the concept of membrane bioreactors (MBRs) in membrane technology has been a reliable and promising technology that has been widely applied in the treatment of domestic and industrial wastewater. This is because of its undisputable and proven advantages such as ease of operation and scale-up, high-quality permeate, small footprint and low capital and operating cost [1,2]. Amidst the MBRs, flat sheet MBR has been reported as one of the main constellations because of its advantages such as good water and wastewater treatment performance, low operating cost and mechanical stability [3,4]. However, membrane fouling which is mainly caused by foulant deposition on membrane surface and pores has been and still remain the primary hindrance of its effective application,

* Corresponding author.

which usually result in increased energy consumption, operation cost, treatment time, excessive chemical consumption, flux declination which promotes filtration resistance and on the long-term, degrade membrane life [5–7]. Several studies in the past have revealed various fouling mechanisms and also proffered possible solutions, by developing measures that can mitigate membrane fouling in MBR application [8–10], and there seems to be a continuous interest of researchers in exploring more possibilities in providing better outcome as regarding membrane technology [7,11].

Chiefly, membrane material used in MBR application is of utmost importance in membrane fouling study and nearly all the ones used for vital industrial applications are made of either inorganic or organic polymers with the latter leading the existing market. Several organic ones such as polyacrylonitrile, poly(ethersulfone), polysulfone, polyimide, polyamide, polypropylene, polyethylene, polytetrafluoroethylene and poly(vinylidene fluoride) (PVDF) have been widely employed in ultrafiltration and microfiltration (MF) wastewater treatment and other applications [12–14], but one of them which have received increasing attention with regards to external shape is the flat-sheet PVDF membrane [15]. Its multifaceted properties such as high mechanical strength and thermal stability, excellent aging, chemical and anti-oxidation resistance, good thermodynamic compatibility in blending, appreciable processability and solubility in common organic solvents have made it an enviable choice [12,16,17].

One of the most efficient and excellent photocatalyst which has found its use in water and wastewater application is titanium dioxide (TiO_2) and this is due to its special properties such as low cost, chemical stability, high photocatalytic activity and non-toxicity [18,19]. TiO_2 photocatalyzed degradation technique is one of the choicest ways for treating wastewater containing organic contaminants, but separating TiO_2 particles during this process is another challenge to be solved in real-life applications because of their fine particle size, which is difficult to be removed by gravity settling [20,21]. To overcome this, some attempts have been made on the separation of TiO_2 particles by various coagulation techniques [21–23] and membrane separation using low-pressure flat sheet membranes [20,24,25]. However, the latter process of removal often results in blockage of the pores by the continuous deposition of the TiO_2 particles on the surface of the membrane thus leading to membrane fouling and secondary pollution [19,26].

To avoid continuous deposition of foulant on the surface of the membrane during MBRs operation, the concept of membrane cleaning (which can be in-situ or ex-situ) has been embraced as a recovery approach in both the engineering and academy community [11]. Several cleaning methods exist but the three most generally recognized ones are physical cleaning, chemical cleaning and combined physical and chemical cleaning methods [27–29]. Unfortunately, the simplicity of the physical cleaning process and its limitation in eliminating thoroughly irreversible foulants, make the chemical cleaning processes more preferable. For effective chemical cleaning of fouled membranes to be achieved, utmost importance must be given to the selection of a suitable cleaning solutions or agents. These agents must possess

the ability to dissolve and remove most (if not all) of the deposited materials on the membrane surface without causing severe damage, which can utterly alter the membrane virgin properties [30,31]. Some cleaning agents include acids, alkalis, surfactants, oxidizing agents, enzymes and metal chelating agents. An example of one of these aforementioned cleaning agents is sodium hypochlorite (NaClO), which is a versatile chemical oxidant that has been widely applied in membrane cleaning owing to its ease of use, availability and low-cost [32]. Most of the irreversible fouling in the membrane could be eliminated by NaClO depending on the membrane material, foulant type and operating conditions [33,34]. Another strong oxidant having the potential of removing foulants from membrane surface is hydrogen peroxide (H_2O_2). Although, less attention has been given to its application in membrane cleaning due to its restriction of reactivity limited by a high activation energy barrier [35]. In addition, the report on its cleaning efficiency provided in literature particularly on its interaction with organic membrane foulant seems unclear.

Sequel to the continuous and usual cleaning of fouled membranes by cleaning agents, it is essential to periodically and strategically check the well-being of membranes during operation (after consistent reduction of performance have been noticed) and most importantly after service life, in order to fully understand the fouling mechanism. This phenomenon is generally described as membrane autopsy or membrane post-mortem. It is a unique way of revealing the cause of membrane damage caused by fouling events in the membrane system by following some guided analytical techniques and procedures. It is also an advantageous way of investigating the nature and characteristics of foulants and their mechanism of occurrence [2,36,37]. A Plethora of research have reported autopsy of some membrane elements applied in water and wastewater treatment, but most of these studies focused mainly on seawater desalination, groundwater desalination and surface water using high-pressure membranes [38–44]. Others reported membrane elements used in processing synthetic wastewater containing common model foulants such as bovine serum albumin, humic acid and sodium alginate, rather than the real wastewater containing various contaminants, and this most often is considered in mild conditions [15,44,45]. Inarguably, there are tendencies that some variance will exist between the properties of real wastewater and mimicked or modeled wastewater owing to their complex constituents; which may have an adverse effect on the membrane and also lead to complicated fouling phenomena. Also, studies which present simple but effective analytical protocol in identifying membrane fouling caused by contained TiO_2 particles wastewater and possible damages during/after membrane service life, especially in the low-pressure membrane are limited. On this note, it is therefore essential to understand the effect of TiO_2 particles and other related contaminant deposition on the low-pressure membrane and its associated fouling mechanism via a simple but systematic membrane post-mortem study. This study, therefore, provides some useful insights into the fouling formation mechanism and chemical cleaning behavior of flat-sheet PVDF-based membrane used in MBR for separating TiO_2 particles and this was achieved

specifically via two main objectives which are: (a) to analyze the foulant composition and fouling formation mechanism of the fouled membrane using a systematic post-mortem analytical procedures of characterization and (b) to assess the membrane cleaning efficiency using DI water, NaClO and H_2O_2 as cleaning solutions in relation to flux recovery.

2. Materials and methods

2.1. Materials

A flat sheet PVDF-based membrane manufactured by a renowned flat-sheet membrane manufacturer in Fujian Province, China was used in separating TiO_2 particles from feedwater in a treatment plant located at Panzhihua, Sichuan Province, China. This membrane was used for approximately seven months (January to July 2020) without cleaning, after which it was severely fouled. The fouled membrane was carefully transported to the laboratory for investigation. Another membrane, produced via a similar operation, which has not been used (designated as 'neat membrane' in this study) was also supplied by the manufacturer. The manufacturer's detail parameter was not supplied as it was considered proprietary. Analytical grade of chemicals used include sodium hypochlorite aqueous solution (NaClO, 10%–12%), hydrogen peroxide (H_2O_2, 30% aqueous solution), pure ethanol (moisture ≤0.3%), hydrochloric acid (HCl, 37% purity), methylene blue solution (0.05 wt.% in water), and sodium hydroxide (NaOH, 100% purity) and were all supplied by Sinopharm Chemical Reagent Co., Ltd., China with the exception of methylene blue solution which was purchased from Sigma-Aldrich (Germany). All the reagents were used as received without further purification and deionized (DI) water with conductivity less than 10 μs cm^{-1} was used for washing and solution preparation throughout the experiments.

2.2. MBR design and operation set-up

TiO_2 particles in raw wastewater were separated using MF membrane as an advanced pretreatment medium. The schematic diagram of the MF pretreatment process is presented in Fig. 1. Prior to being pumped to the MBR, the wastewater was stored in a feed tank. The bioreactor in the system consisted of an acrylic tank, in which a flat sheet MF membrane with a mean pore size of 0.2 μm and an area of 0.12 m^2 was vertically immersed. A small space of about 15 mm was set between the wall of the reactor and the membrane for proper scouring of the membrane via the flow of air. Aeration and backflush were introduced at an air rate of 7 L min^{-1} to drive the permeate sucked from the raw wastewater tank by constant flow pumps and to mitigate fouling. Pressure transducers were used to monitor the transmembrane pressure (TMP) at about 25 kPa. Other accessories such as airflow control valve, liquid level sensor and system data acquisition software were connected to the MBR system. The membrane was continuously used without cleaning. After some months of operation, the membrane elements were fouled and their performance was reduced. They were then autopsied by transporting them to the laboratory to study the fouling composition and mechanism.

2.3. Experimental procedures

2.3.1. Water quality and constituent analysis

TiO_2 feed water was collected in a guided plastic container which had been thoroughly washed with disinfectants and deionized water prior to collection. To preserve and maintain its original properties, the feedwater was transported in an ice chest to the laboratory and thereafter kept in the refrigerator prior to analysis. The feedwater sample was analyzed in accordance with the standard methods for the examination of water and wastewater [46].
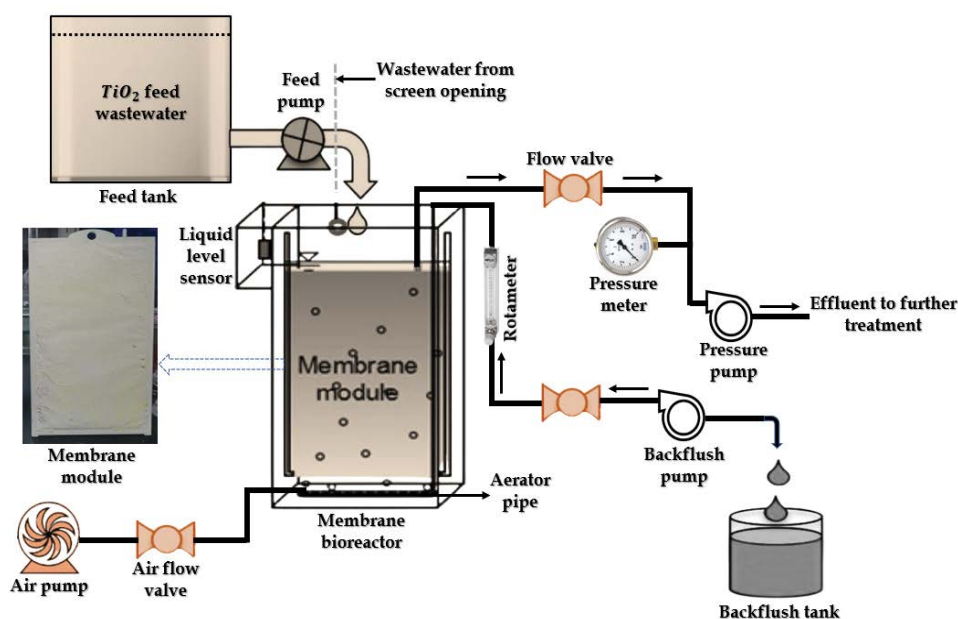

Fig. 1. Schematic diagram of the MBR set-up and operation.

The pH was measured using a portable pH meter (Beckman 260, Fullerton, CA), conductivity measurement was taken with sensION+EC5, Hach, turbidity was measured by a turbidity meter (Hach 2100AN, Colorado, USA). Before chemical oxygen demand (COD) measurement, the feedwater was filtered through a 0.45 μm membrane filter. COD was measured using Hach DRB 200, (Colorado, USA) and Hach DR 900, (Colorado, USA) for digesting and measuring respectively. The concentrations of the elements were quantified with an inductively coupled plasma–optical emission spectrometer (Perkin Elmer, Optima 7000 DV, Waltham, USA). The summary of the characteristics of the feedwater is presented in Table 1.

2.3.2. Foulant constituent's analysis

Foulant in form of a cake layer on the membrane surface was gently extracted using a light plastic plate. Before extraction, the plate was cleaned with absolute ethanol, rinsed with DI water and then dried. Thereafter, the accumulated foulant was characterized by attenuated total reflectance–Fourier-transform infrared spectroscopy (ATR–FTIR), scanning electron microscopy (SEM) and energy-dispersive X-ray (EDX) spectroscopy in order to comprehend the underlying mechanism of the membrane fouling. Other tests such as chemical solubility test and surface density were also performed and their detailed explanation is provided in supporting information.

2.3.3. Membrane sample preparation and analysis protocol

Upon reception of the fouled membranes, they were gently taken out of a guided waterproof box using a clean glove to prevent any further contamination and damage. At first, representative membranes were visually inspected for visible damages and cracks/fractures. Afterward, they were systematically cut into uniform coupon sizes [47] before commencing the experiment. Three sampling positions were selected on the representative fouled flat sheet membrane element to represent the top (T), middle (M) and bottom (B) section for adequate analysis. For the neat membrane, spots were randomly selected and cut for testing. The schematic diagram of the sample preparation is provided in Fig. S2. The prepared membrane samples were then analyzed using a systematic post-mortem analysis protocol (Fig. 2) for proper investigation.

2.3.4. Fouled membrane characterization

In line with the adopted post-mortem analysis protocol in Fig. 2, analytical tests including chemical, mechanical/integrity and physical properties of the fouled membrane were characterized alongside the neat membrane for comparison. The membrane surface morphologies were examined under a field emission scanning electron microscope (FESEM, Hitachi S-4800, Japan) at an accelerating voltage of 5–10 kV. Prior to the examination, the samples were fastened on tape placed on an aluminum metal holder and then splashed with a thin layer of gold to prevent or reduce charging reduction under the electron beam of the machine. The relative elemental composition of the membranes was detected using an EDX spectrometer attached

Table 1
Characteristics of the raw TiO_2 feedwater

Parameters	Values
pH	2.15 ± 0.12
Temperature, °C	24.5
Turbidity, NTU	$1{,}383 \pm 4.54$
Conductivity, μs cm^{-1}	$3{,}820 \pm 14.14$
COD, mg L^{-1}	13,110
Chlorine (Cl), mg L^{-1}	750
Sodium (Na), mg L^{-1}	1,810
Potassium (K), mg L^{-1}	420
Calcium, mg L^{-1}	480
Aluminum (Al), mg L^{-1}	1,630
Iron (Fe), mg L^{-1}	16,300
Magnesium (Mg), mg L^{-1}	1,770
Silicon (Si), mg L^{-1}	17,700
Titanium (Ti), mg L^{-1}	54,230
Sulphur (S), mg L^{-1}	13,330
Phosphorus (P), mg L^{-1}	540
Manganese (Mn), mg L^{-1}	510

to the FESEM machine. The FTIR spectroscopy (Nicolet 6700 FTIR, Thermo Fisher Scientific Inc., USA) was used to investigate the present functional groups on the membranes. Spectra were acquired using OMNIC software at a resolution of 4 cm^{-1} and 32 scans per spectrum within a wave number range of 4,000–400 cm^{-1}, using the ATR method. X-ray diffraction (XRD, X'Pert Pro PANalytical, The Netherlands) was used to characterize the crystallographic phases of the membranes. This was achieved by gently placing the membrane sample on Plexiglass and thereafter placing it on the diffractometer. Scanning was achieved from $5 < 2\theta < 90$ with a scanning step of 0.02° with the generator set at 40 kV and 40 mA. Zeta potential of the membranes was measured with a streaming potential analyzer (SurPASS 3, Anton Paar, Australia) having an automatic titrating assemblage, containing 0.010 mol L^{-1} KCl electrolyte solution. The pH was adjusted from 3–11 using a flowing liquid of 0.05 mol L^{-1} HCl and NaOH solution at room temperature of 23°C ± 2°C, with gap height of approximately 100 ± 5 μm maintained all through the test. Eq. (1) was used to compute the surface zeta potential based on Helmholtz–Smoluchowski equation and three values were averaged. The membrane's adhesion and hydrophilicity properties were analyzed by a contact angle analyzer (DSA100, Krüss, German). Prior to testing, membrane samples were sliced into the desired size and taped on a flexible Plexiglass. Using DI water as the reference solvent of measurement, 3 μL of DI water was dropped from a microsyringe with a stainless-steel needle on the membrane surface at room temperature. The contact angle was immediately measured after placement and five measurements were taken for each sample at various points for averaging. Membrane porosity was determined by the gravimetric method while its tortuosity was estimated from the porosity. The thickness was also measured using a digital micrometer (293-252, MITUTOYO, Kanagawa,
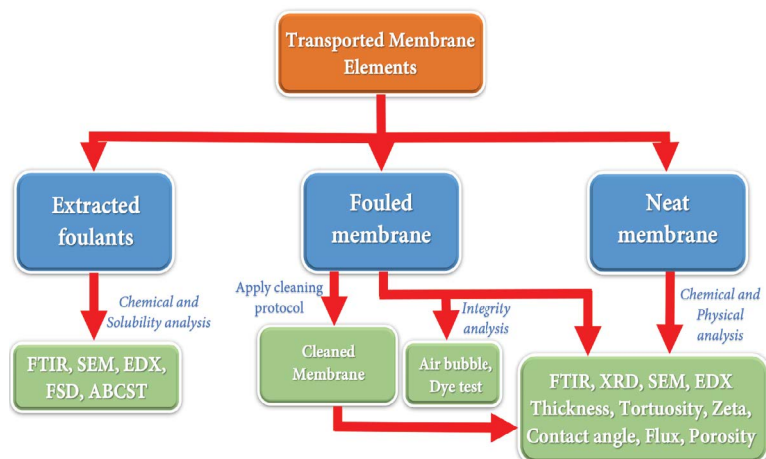
Fig. 2. Schematic diagram of the membrane post-mortem analysis protocol.
Note: FSD and ABCST means foulant surface density and acid-base chemical solubility test respectively.

Japan), with a precision of ±0.01 mm. Ten points were randomly selected on each membrane and their mean and standard deviation are reported. Detailed measurement procedures for the porosity, tortuosity and thickness calculation equation are given in previous reports [17,48]. The air bubble test was achieved on the membrane surface by introducing air pressure of about 0.02–0.030 MPa into permeate tube and the membranes are then monitored for the escape of air bubbles. A dye test was conducted following the procedure of [47] to verify the presence of microstructural damage on the fouled membranes.

$$\zeta = \frac{dU}{dP}\frac{\eta}{\varepsilon\varepsilon_0}K \tag{1}$$

where U is the streaming potential, P is the pressure, η is the viscosity of the electrolyte solution, ε is the dielectric constant of the electrolyte solution, ε_0 is the vacuum permittivity and K is the electrolyte conductivity.

2.3.5. Membrane cleaning protocol and evaluation

To investigate the recovery rate of the fouled membrane, a one-time chemical cleaning method was employed using DI water, NaClO and H_2O_2 as cleaning agents. The effects of these cleaning solutions on the fouled membrane were investigated. Firstly, the fouled membrane was embedded in the prepared concentrated cleaning solution. Two concentrations were selected each for NaClO and H_2O_2 based on previous reports [35,49,50]. The selected volume concentration for NaClO is 1.5% and 3% while for H_2O_2 is 0.5% and 1.5%. The static soaking time in both solutions is 12 h. Similarly, fouled membranes were also soaked in slightly warm DI water maintained at a temperature of 30°C ± 1°C. After the completion of the embedding period, the membranes were altogether gently removed and rinsed with DI water in order to allay the chemical effect and remove residue of the cleaning agents prior to further testing. The cleaned membranes were characterized for FTIR, XRD, SEM, EDX, surface charge, surface hydrophilicity, porosity

and thickness as described in Section. 2.2.4 and their results were compared with the neat and fouled membranes.

2.3.6. Membrane filtration process and cleaning efficiency

The permeation performance of the neat, fouled and cleaned membranes was evaluated using both the dead-end (Model 8010, Millipore Corp., Burlington, MA, USA) and cross-flow filtration units (Memb-flow model, USA). The dead-end filtration cell has an effective membrane area of 12.56 cm² and prior to measurement, the membranes were pre-stressed with DI water for 30 min at 0.15 MPa in order to achieve a steady flux. The permeate flux was then tested at a TMP of 0.10 MPa for 10 min. In the same vein, the cross-flow filtration unit has an effective membrane area of 8.4 cm² and a cross-flow velocity of 0.2 m s⁻¹. Before commencement of measurement, each membrane was pre-stressed for 30 min at 0.20 MPa to get a stable flux, the permeate was then collected for 10 min at 0.10 MPa. The permeation flux for the fouled (J_{FM}), cleaned (J_{CM}) and neat membranes (J_{NM}), (in L m⁻² h⁻¹) were calculated by Eq. (2). In addition, the cleaning efficiency was determined with the recovery of pure water flux via the cleaned membrane and was estimated as given in Eq. (3).

$$\left(J_{FM\,or\,CM\,or\,NM}\right) = \frac{V}{A\times\Delta t} \tag{2}$$

$$\text{Cleaning Efficiency}(\%) = \frac{J_{CM}-J_{FM}}{J_{NM}-J_{FM}}\times 100 \tag{3}$$

where V is the volume of permeated water (L), A is the effective membrane area (m²) and Δt is the permeation time (h).

3. Results and discussion

3.1. Foulant characterization analysis

The foulant was examined under the FESEM machine at magnifications of both 1,000× and 5,000× and EDX was used to obtain their elemental composition. The result of
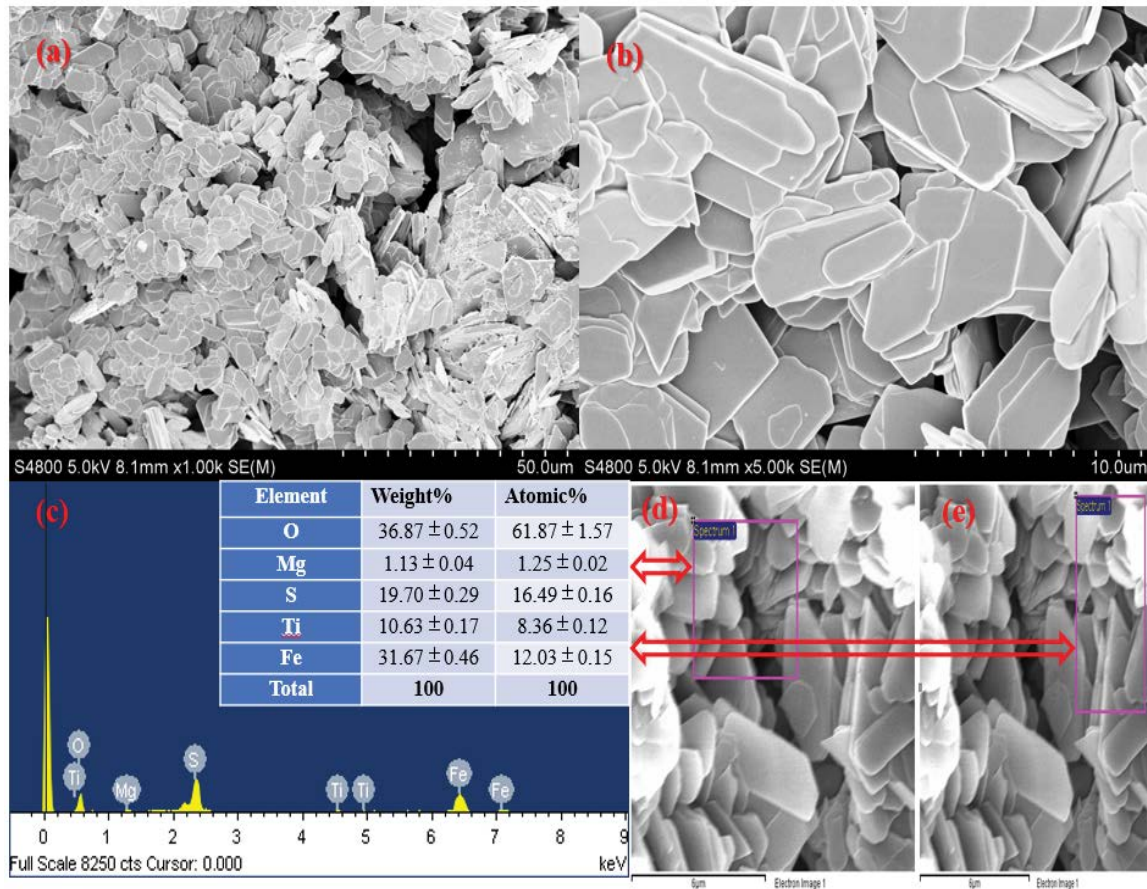
Fig. 3. Foulant (a) SEM image at 1,000× magnification, (b) SEM image at 5,000× magnification, (c) EDX spectra and average element composition and (d, e) EDX typical elemental sites acquired for analysis.

the analysis is presented in Fig. 3. The weight and atomic percentage recorded are the average of points taken during the analysis. The results of the SEM-EDX analysis of the foulants indicate that O (~37% by weight) and Fe (~32% by weight) are the two major foulants with S, Mg and Ti making up the other elements. As revealed in the detailed analysis result of the EDX, the O and S were compounded with Si, Fe and Mg to form silicon dioxide (SiO_2, known as silica), iron disulfide (FeS_2, known as pyrite) and magnesium oxide (MgO) respectively. SEM images further validate the presence of these compounds which show several rod-like with well-defined shapes having a triangular, pentagonal and rhombohedral crystalline structures with sharp edges (Fig. 3a and b). The shapes of FeS_2, SiO_2 and MgO have been reported in previous literature [51–53]. Furthermore, Fe, Mg and S are also seen as part of the major constituents of the feedwater analysis (Table 1). Generally, foulants (especially Fe and Si) when deposited on the surface of the membrane even in a small quantity, have great tendencies of reducing the membrane life [43]. In addition, the FTIR spectra of the foulant are presented in Fig. 4. As shown, the characteristics band peaks were detected at 2,350; 1,790 and 1,028 cm^{-1} representing C–O stretching ($CaCO_3$), 1,088 cm^{-1} representing symmetric stretching of Fe–S (FeS_2) and 583–414 cm^{-1} representing symmetric stretching of

Si–O (SiO_2). The broad peak in the range 3,100–3,500 cm^{-1} indicates the presence of MgO constituents in the foulant [54,55]. This result further validates the elemental composition revealed by the EDX analysis, Although, $CaCO_3$ was not captured by the EDX analysis, it was visibly acquired by the FTIR analysis. The chemical solubility analysis (supporting information) also revealed the presence of some elements which was observed through gas evolution and color change when dissolved in acid and base.

3.2. Membrane characterization analysis

3.2.1. SEM and EDX analysis

The surface morphology of the neat, fouled and cleaned membranes characterized using the FESEM machine at magnifications of 5,000× is presented in Fig. 5. As observed, the fouled membrane was completely covered by the foulant but none was found on the surface of the neat membrane, as it was defect-free (Fig. 5a and b). When cleaned with DI water, a good degree of membrane surface recovery was achieved but there was some deposition of the foulant left on the membrane surface (Fig. 5c), which were stubborn and could not be easily removed with DI water. In the same manner, the fouled membrane cleaned with 1.5 M NaClO shows some areas of the membrane
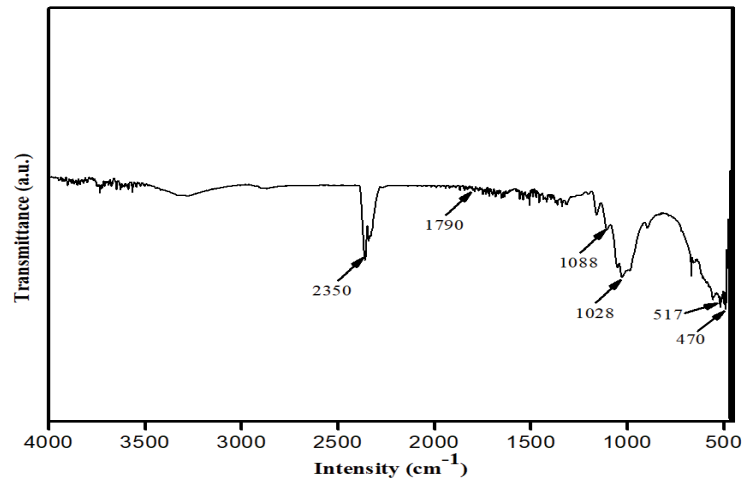
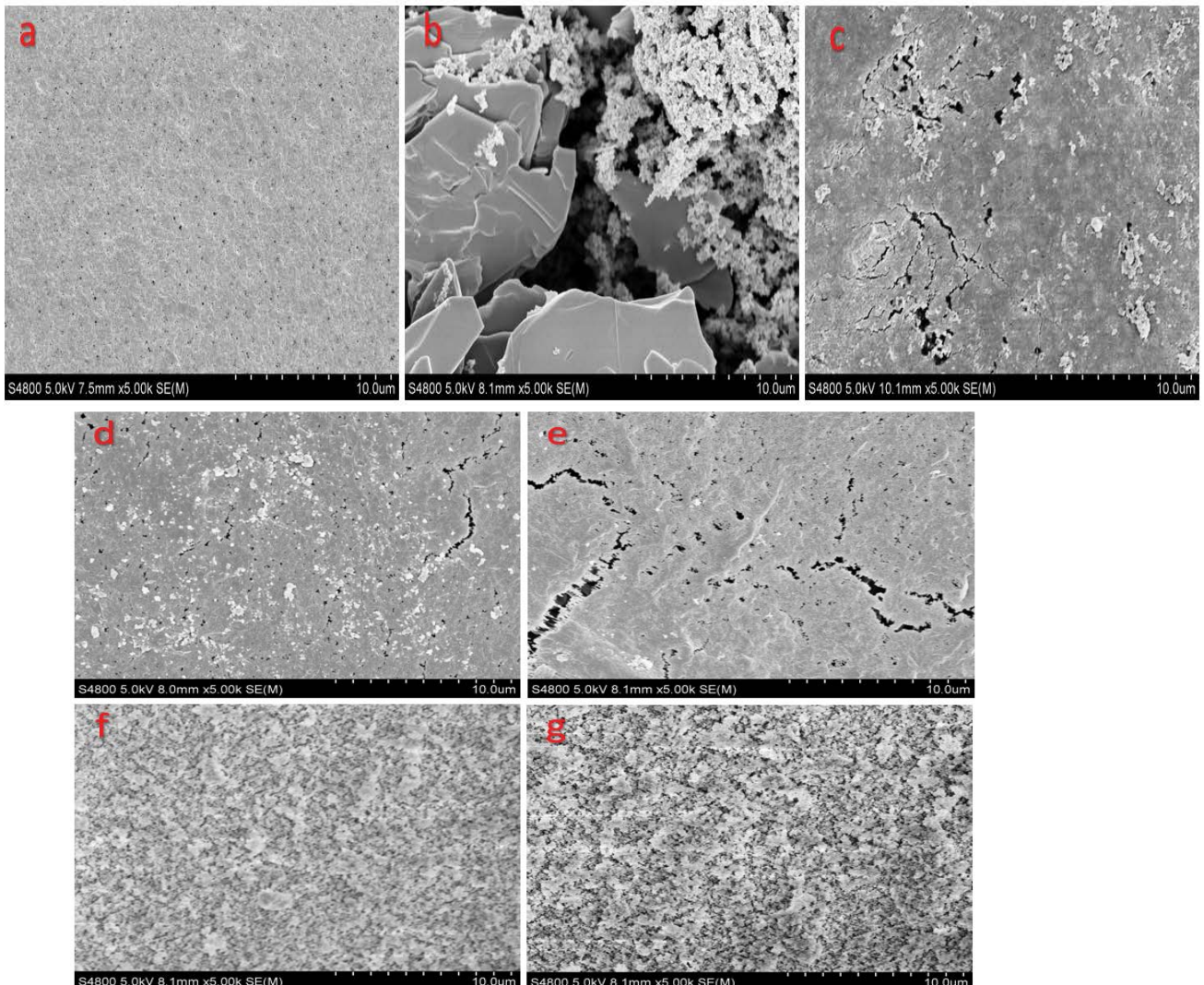Fig. 4. FTIR spectra of the foulant.

Fig. 5. SEM images of the (a) neat membrane, (b) fouled membrane, (c) DI water cleaned membrane, (d) 1.5 M NaClO cleaned membrane, (e) 3 M NaClO cleaned membrane, (f) 0.5 M H_2O_2 cleaned membrane, and (g) 1.5 M H_2O_2 cleaned membrane.

surface still covered by minor deposition of the foulant (Fig. 5d) but none was visibly seen on the surface of the membrane cleaned with 3 M NaClO (Fig. 5e). The foulants were weakened with their polymeric chains decomposed into minute fragments by the NaClO. Although, the membranes were observed to suffer some degradation in the process by the action of the NaClO [33], which was more severe at 3 M of the cleaning solution (Fig. 5d and e). It has been established that NaClO, though effective in removing most inorganic and organic foulants, has the potential to degrade the membrane mechanical strength and alter its physicochemical properties [49]. Likewise, the fouled membrane cleaned with 0.5 M and 1.5 M of H_2O_2 tends to show appreciable removal of foulant, as their surfaces look rough and porous (Fig. 5f and g). Nevertheless, the membrane suffers some intense degree of degradation. Compared to the membranes cleaned with NaClO, H_2O_2 cleaned membrane surfaces were defected thus reflecting the strong oxidative power of H_2O_2.

The elemental composition of the neat, fouled and cleaned membrane elements were obtained from EDX spectra and the results are presented in Fig. 6. As clearly shown, the main constituent elements observed in the spectrum of the neat membrane are carbon (C) and fluorine (F) (which are the main elements existing in polymeric PVDF chains) but with a small amount of oxygen (O) which could results from contamination during experimental work (Fig. 6a). However, the constituent elements observed in the spectrum of the fouled membrane are carbon (C), oxygen (O), aluminum (Al), silicon (Si), sulfur (S), titanium (Ti) and iron (Fe) (Fig. 6b). The weight and atomic percentage of element C were drastically reduced to only ~ 4% and 7% respectively while element F was not detected at all thus reflecting the severe coverage of the foulants deposition on the membrane. Element O was also abundantly detected with weight and atomic percentage of ~ 64% and 77% respectively. This may result from the presence of the hydroxyl groups contained in the foulant and attached to elements such as Si and Ti. This thus reveals the pore blocking of the membrane caused by the cake deposition during separation. Moreover, the amount of S, Fe, Ti, Si and Al in the spectrum were also significant as they contribute to the overall fouling mechanism of the membrane. After cleaning the fouled membrane with DI water and NaClO solutions, element F was recovered and C increased while O significantly diminished. Also, the composition of other elements such as Mg, Ti and Fe reduced while S and Si were successfully eliminated (Fig. 6c–e). For membranes cleaned with H_2O_2, the spectra revealed the removal and reduction of elements such as Al, S, Ti and Fe but could not seems to eliminate O and Si, rather they were refouled with them (Fig. 6f and g).

3.2.2. FTIR and XRD analysis

To reveal the change in the chemical groups and functional structures caused by deposited and absorbed particles on the neat, fouled and cleaned membrane surfaces, ATR–FTIR set in transmittance was employed and this was accomplished using peak spectrum. The acquired spectra are given in Fig. 7. From the spectra, the neat membrane displayed the typical characteristic band peaks of PVDF indexed to α-phase located at 615, 763 and 795 cm^{-1} all representing CF$_2$ bending and stretching vibration while the band peaks located at 975 and 1,070 cm^{-1}, represent CH$_2$ rocking [17,56]. The band peaks located at 840; 1,033; 1,275 and 1,404 cm^{-1} are bands corresponding to β-phase representing skeletal C–C stretching and CH$_2$ rocking [57], CF$_2$ stretching [57,58] and CH$_2$ stretching [59,60] respectively. Furthermore, band peaks noticed at 2,930 and 2,967 cm^{-1} represent CH$_2$ symmetric and asymmetric stretching vibration modes [61] while at band peak 1,454 cm^{-1}, there was deformation of CH$_2$ groups. The spectrum acquired for the fouled membrane shows a drastic reduction in the transmittance intensity when compared to the neat membrane, as it takes a flat/straight-line form. This spectrum is somewhat expected as the fouled membrane surface was covered by the foulants, thus overlying the vibration of the membrane during spectra acquisition [62]. Moreover, the spectra acquired for the DI water cleaned, NaClO (at 1.5 and 3 M) cleaned and H_2O_2 (at 0.5 and 1.5 M) cleaned membranes revealed a similar pattern with the neat membrane indicating a good recovery, as there were no notable differences from 500 to 4,000 cm^{-1} except some few bands' adjustments noticed between broad absorption band peaks of 2,500 and 3,600 cm^{-1}. Also, the effect of the cleaning agents on the membrane was noticed in the rocking, wagging and deformation of band peaks as observed in their spectra.

XRD analysis was employed to investigate the crystalline structure of the neat, fouled and cleaned membranes and to see if there are noticeable changes as shown in Fig. 8. The existence of PVDF polymers can be seen generally in five crystalline forms namely α, β, γ, δ and ε phases [14,63] but it is basically and mostly noticed in the first three major phases out of the five [64]. From the figure, it can be noticed that the neat PVDF membrane exhibits two crystalline characteristic peaks at 17.86° and 26.02° (representing diffractions in crystallographic planes 020 and 021) which are both attributed to the α-phase while a third characteristic peak at 20.66° (representing diffraction in crystallographic plane 110) is indexed to the β-phase. In the fouled PVDF membrane, a strong peak at 9.81° (indicated in light green circular symbol) was observed while other weak peaks at 9.81°, 14.49°, 22.13° and 28.85° were also noticed. These peaks are envisaged to be caused by the interaction between the PVDF polymer and the deposited constituent of the foulants (such as Ti, Fe, Si, Al) on the surface of the membrane which influenced the polymer crystal structure during phase transition [65]. Furthermore, similar crystalline characteristic peaks were observed in all the cleaned membranes as seen in the neat membrane. Although, some insignificant shifts were detected in their characteristic peaks using XRD pattern analysis software. These characteristics peaks are recorded in Table S3. This further attests to the fact that the cleaning solutions (especially NaClO and H_2O_2 at higher concentrations) were effective in recovery the membranes but with some intrinsic changes in the hydrophilicity, surface charges and flux as explained in later sections.

3.2.3. Visual examination

As a vital step in membrane fouling investigation, the membrane components transported from the wastewater
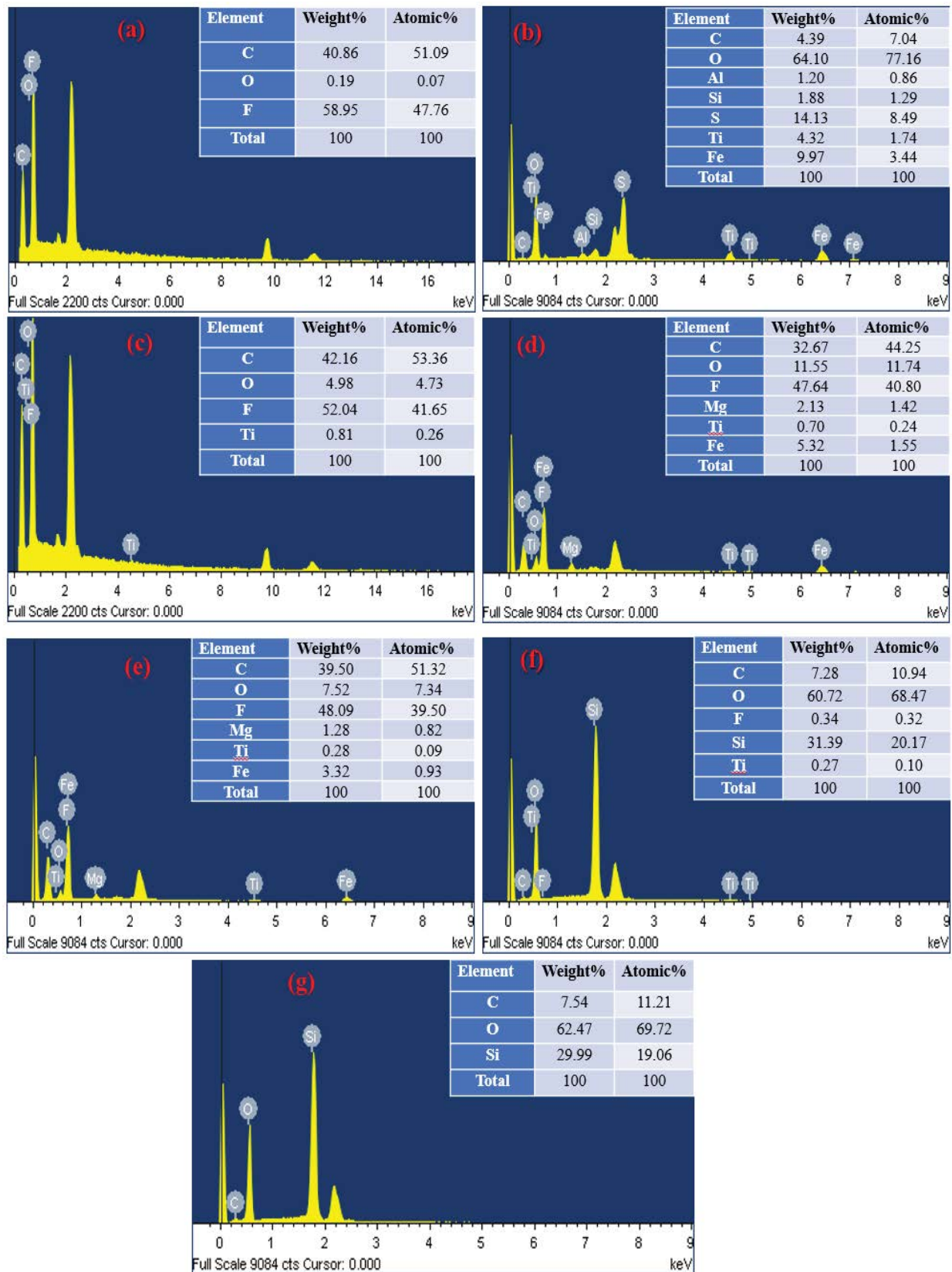
Fig. 6. EDX spectra and element composition of (a) neat membrane, (b) fouled membrane, (c) DI water cleaned membrane, (d) 1.5 M NaClO cleaned membrane, (e) 3 M NaClO cleaned membrane, (f) 0.5 M H_2O_2 cleaned membrane, and (g) 1.5 M H_2O_2 cleaned membrane.
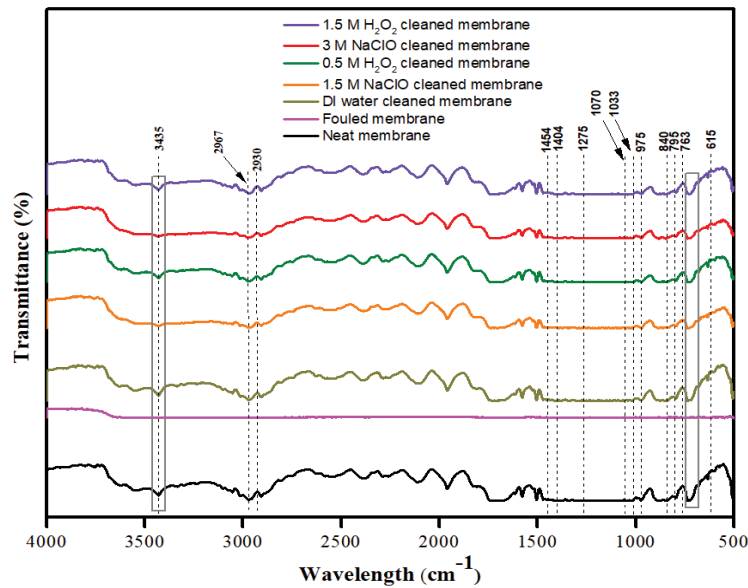
Fig. 7. ATR–FTIR of neat, fouled, DI water cleaned, NaClO cleaned and H_2O_2 cleaned membranes.

plant was visually examined internally and externally in order to check for physical cracks, embossments, scales, flaws, blistering and extent of fouling on the surface of the membrane layer, the permeate carriers, feed spacers and the membrane leaves. As shown in Fig. 9, the surface of the fouled flat sheet membrane element was widely spotted with foulant having light grey color in some regions and dark grey in others (Fig. 9a1 and a2). The feed spacer and the permeate carrier had no visible stain of the foulant on them (Fig. 9b1 and b2). In addition, the fouled membrane element extracted from the membrane module has its surface covered with grey spots, indicating the foulant (Fig. 9c1). These grey spots were easily cleaned off when soaked and washed with DI water. Nevertheless, some irregular transparent light brown was left on the surface of the membrane (Fig. 9c2). The cleaning of the fouled membrane with 1.5 M and 3.0 M NaClO changed their colors to light and dark reddish-brown respectively (Fig. 9d1 and d2) indicating the presence of Fe as one of the major constituents of the foulant. Moreover, no visible cracks or defects were observed on the surfaces of the membrane. In contrast, some slight embossments were noticed on the surface of the membrane cleaned with 0.5 M H_2O_2 which were more severe on the membrane cleaned with 1.5 M H_2O_2, even though the cleaning solution was physically effective in removing the foulant from the surface of the membrane (Fig. 9e1 and e2). In sum, no permanent physical damage was observed on the surfaces of the cleaned membranes, feed spacers and membrane leaves.

3.2.4. Dye and air bubble test

The dye and air bubble test was used to verify the integrity and strength of the membrane to check if there is any structural damage done to the membrane during operation in the MBR plant. Prepared methylene blue solution was randomly dropped without any pressure applied on

the surface of two membrane coupons, which were initially placed on a flat platform prior to testing. The result (Fig. S3) shows that the fouled membrane had suffered some slight microstructural damage during operation as traces of methylene blue solution were seen on the permeate sides of tested membrane elements (M1 and M2). In the same manner, the air bubble test indicates that the membrane had suffered some microstructural damage during operation, as air bubbles were seen escaping via some sections of the membrane when air pressure was applied. It is envisaged that this structural damage could be a result of long exposure of the membrane to the wastewater which exhibits a low pH (Table 1). As reported in our previous work, PVDF-based membranes exposed to the region of low pH for an extensive period of time could suffer some structural damage which will evidently affect their mechanical properties [48].

3.2.5. Thickness, porosity and tortuosity

The thickness and porosity of a membrane are two key parameters that provide a clear understanding of the flux and integrity characteristics a membrane will potentially exhibit. Table 2 presents the thickness and porosity of the neat, fouled and cleaned membranes with their respective standard deviations. It was essential to measure the thickness of the fouled membrane to know the degree of foulant deposition and distribution on the membrane. The thicknesses of the neat and fouled membranes which were randomly measured at different points of the extracted membrane coupons are 202.7 ± 2.21 μm and 220.6 ± 6.40 μm respectively. This result reveals that some deposition of the foulant was firmly stuck to the surface of the membrane which thus increases its thickness. This was also confirmed by the visual examination representation in Fig. 9. Undoubtedly, the cleaning of the fouled membrane with DI water and different
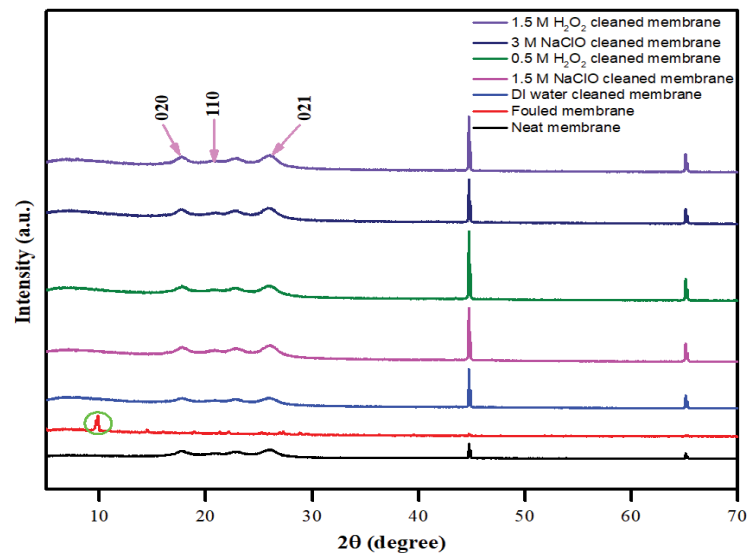
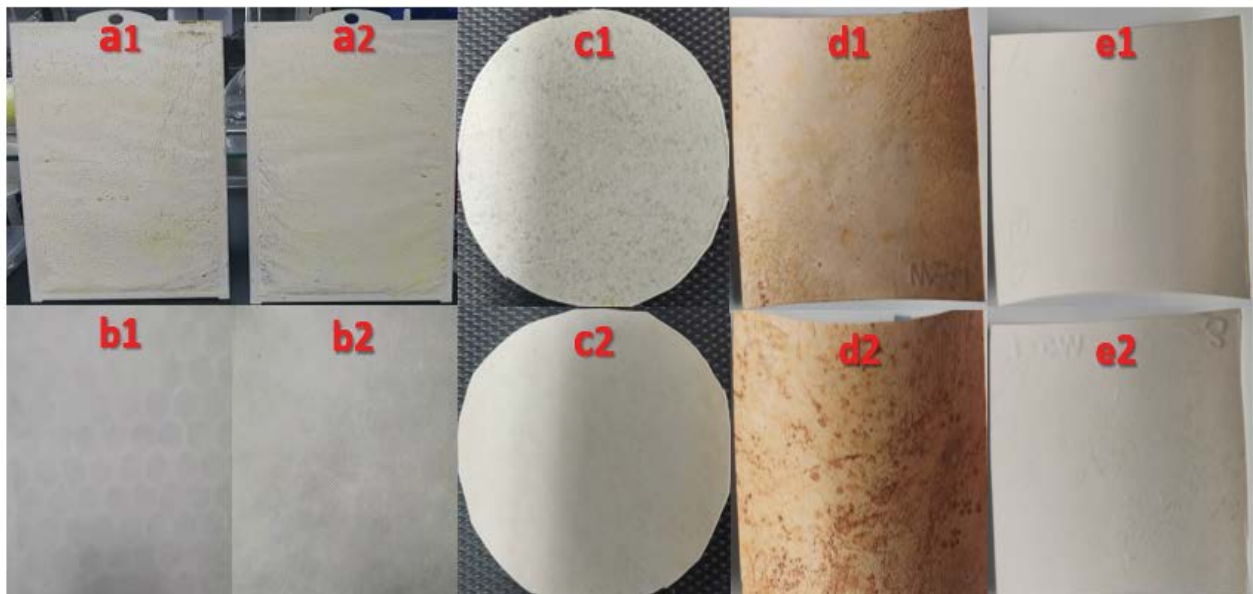Fig. 8. XRD crystalline phase of neat, fouled, DI water cleaned, NaClO cleaned and H_2O_2 cleaned membranes.

Fig. 9. Visual inspection of the membrane elements (a1, a2, b1, b2), fouled and DI washed membrane (c1, c2), NaClO cleaned membranes (d1, d2) and H_2O_2 cleaned membranes (e1, e2).

Table 2
Thickness, porosity, tortuosity and contact angle of the neat, fouled and cleaned membranes

Membrane type	Thickness (μm)	Porosity (%)	Tortuosity	Contact angle (°)
Neat	202.7 ± 2.21	66.64 ± 0.45	2.69 ± 0.10	80.1 ± 0.62
Fouled	220.6 ± 6.40	53.42 ± 2.87	4.04 ± 0.39	57.5 ± 2.17
DI water	210.7 ± 1.70	71.05 ± 0.33	2.34 ± 0.07	25.2 ± 3.54
NaClO @ 1.5 M	195.4 ± 1.39	74.03 ± 0.64	2.14 ± 0.04	17.0 ± 1.84
NaClO @ 3 M	194.4 ± 1.27	74.11 ± 1.05	2.14 ± 0.06	15.6 ± 2.72
H_2O_2 @ 0.5 M	198.3 ± 1.60	78.68 ± 0.32	1.87 ± 0.03	12.9 ± 1.34
H_2O_2 @ 1.5 M	196.6 ± 0.98	78.49 ± 0.35	1.88 ± 0.05	12.3 ± 0.97

concentrations of NaClO and H_2O_2 slightly affect the thickness of the membrane thus resulting in reduction, but no remarkable influence on the physical structure of the membrane matrix was noticed. This outcome is in agreement with the findings of [49]. Meanwhile, the porosity of the membranes exhibits a similar pattern of result, but in the opposite direction. The neat and fouled membrane has a porosity of 66.64% ± 0.45% and 53.42% ± 2.87% respectively while the cleaned membrane porosity gradually increases in the order DI water cleaned <1.5 M NaClO cleaned <3 M NaClO cleaned <0.5 M H_2O_2 cleaned <1.5 M H_2O_2 cleaned as given in Table 2. The cleaning of the membrane results in flux and contact angle increments which are discussed in later sections. The tortuosity of the neat, fouled and washed membranes were further estimated from the porosity. It is an important parameter used in revealing the ruggedness and ability of the membrane to withstand extreme conditions. It has an inverse relationship with porosity [66]. The tortuosity of the neat membrane is 2.69 ± 0.10 as shown in Table 2. Meanwhile, the tortuosity of the fouled membrane increased by approximately 1.65 times the neat membrane. This result is expected as the porosity of the fouled membrane is reduced due to membrane pore blocking caused by the foulant. In addition, the tortuosity of the cleaned membranes decreases as their porosity increases, but they still fall within the permissible limit of tortuosity ≥1 proposed by Matyka et al. [67].

3.2.6. Surface charge and hydrophilicity analysis

One of the most important parameters useful in supplying information about the membrane surface charge is the zeta potential. It helps to better understand the membrane retention mechanism and fouling properties of the fouling processes [68,69]. Fig. 10 presents the surface zeta potential analysis of the neat, fouled and cleaned membranes. As shown, the zeta potential of the neat membrane

at pH range 3 to 11 shows a pattern that is similar to polymeric PVDF membranes thus having a zeta potential of −14.27 ± 0.68 mV at neutral pH 7. Furthermore, all the membranes with the exception of the fouled and the H_2O_2 cleaned membranes, exhibited similar surface charge trends as they become more negatively charged with pH increment. For the fouled membrane, the positive zeta potential value of 2.70 ± 1.23 mV at pH 3, which further transit to become negatively charged with increasing pH, could be attributed to the deposition of the foulant on the surface of the membrane. This could be further explained by the electrostatic interaction existing between the foulant and the charge on the membrane surface which is not the same case for the neat membrane. This is a critical factor to consider because, there will be a reduction in fouling propensity on the membrane surface when their zeta potential is more negative, due to the electrostatic repulsion between the foulant and the membrane's surface [70]. In addition, the zeta potential of the NaClO cleaned membranes (for 1.5 M and 3 M) were found to be more negatively charged when compared with those cleansed with DI water and H_2O_2 (for 0.5 M and 1.5 M) particularly at a pH range of 3–7. This observation is similar to the findings of [35]. As observed from the same Fig. 10, there was no significant difference in the zeta potential of all the membranes at a pH range of 9–11, as they tend to falsely plateau without any further significant change but with the exception of the fouled membrane, which displayed an abrupt declination throughout the pH range considered. Generally, it was evident from the analysis that the zeta potential of the membranes is influenced by pH change as they expressly exhibit an inverse relationship.

Similar to zeta potential parameter, surface hydrophilicity of membrane also has a significant effect in controlling or assessing membrane fouling both in bench-scale and pilot-scale of membrane bioreactor system and this can be achieved by measuring the water contact angle of the
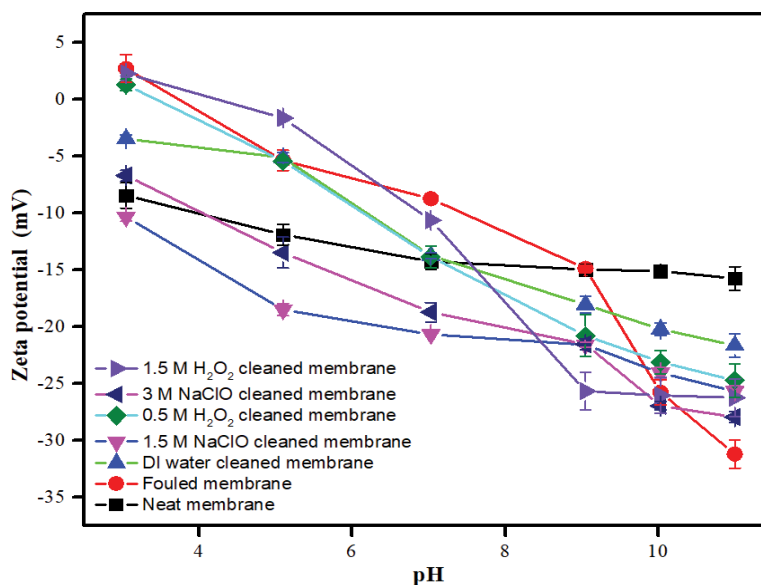

Fig. 10. Surface zeta potential as a function of pH for neat, fouled and cleaned membranes.

membrane material. The contact angles of the neat, fouled and cleaned membranes were measured and the average values are presented in Table 2. The neat membranes exhibited a contact angle of 80.1° ± 0.62° thus revealing the hydrophobic property of the PVDF membrane. It has been established that contact angle values ranging from 0° to 80° represent hydrophilic surfaces while those from 81° to 180° correspond to hydrophobic surfaces [62,71]. For the fouled membrane, a significant reduction was recorded in the contact angle, which was caused by the marked constituent of the foulant as seen in Fig. 5b spreading over the surface of the membrane, thus making it hydrophilic owing to its hydroxyl properties [72]. Similarly, there was a drastic reduction in the contact angles of the cleaned membranes in the decreasing order of DI water cleaned >1.5 M NaClO cleaned >3 M NaClO cleaned >0.5 M H_2O_2 cleaned >1.5 M H_2O_2 cleaned, thus making the membrane more hydrophilic. This is believed to be caused by the segregation of the PVDF polymer chain on the membrane surface membrane during cleaning, as there was the rapid spread of the water droplet on the membrane surface during testing. This has been reported to be caused by electrostatic interactions and the likely presence of hydrogen bonds of the cleaning constituent [73].

3.2.7. Permeation flux and cleaning efficiency

To further understand the fouling formation on the membrane element and the chemical removal efficiency, the results of the water permeation flux of the neat, received fouled and cleaned membranes evaluated using cross-flow and dead-end filtration cell, alongside the cleaning efficiency of the cleaned membranes is presented in Fig. 11. For the result of the cross-flow filtration unit as shown in Fig. 11a, the permeation flux of the neat membrane is 1,465.5 ± 36.48 L m⁻² h⁻¹ which is relatively moderate for low-pressure PVDF membranes, but there was a drastic reduction for that of the fouled membrane, having 164.2 ± 20.58 L m⁻² h⁻¹ as the resulting permeation flux, which is almost one-tenth of the neat membrane. This significant reduction is a result of the massive covering and blockage of the membrane surface and pores by the foulant as revealed by the SEM images in Fig. 5, thus reducing the permeation of water through the membrane. The previous study has reported the permeation flux of the membrane to be greatly influenced by both pore size and surface porosity [49]. Moreover, the permeation flux of membrane cleaned with DI water raised to 631.2 ± 25.07 L m⁻² h⁻¹ while permeation flux of those cleaned with different concentrations of NaClO and H_2O_2 increased relatively from 1,023.5 ± 45.99 to 1,212.7 ± 70.79 L m⁻² h⁻¹ and 1,054.4 ± 55.73 to 1,139.6 ± 8.13 L m⁻² h⁻¹ respectively. The permeation flux of all the membranes tested using a dead-end filtration unit as shown in Fig. 11c followed a similar trend with that of the cross-flow filtration system. The neat and the fouled membranes have permeation fluxes of 1,148.5 ± 53.69 and 405.1 ± 15.02 L m⁻² h⁻¹ respectively while the DI water cleaned membrane has the least among the washed membranes to be 544.1 ± 41.46 L m⁻² h⁻¹. Justifiably, this result trend is similar to that of the contact angle given in Table 2, which reveals the hydrophilicity nature of the membrane with increasing concentration of the cleaning agents. In addition, their membrane cleaning efficiency (i.e., pure water flux recovery) was evaluated. For the cross-flow filtration unit result (Fig. 11b), the membrane cleaned with 3 M NaClO has the highest cleaning efficiency (81%), followed by the membrane cleaned with 1.5 M H_2O_2 having a cleaning efficiency of 75%. The cleaning of 1.5 M NaClO and 0.5 M H_2O_2 cleaning was just a bit different from each other with approximately 2% while the DI water cleaned membrane has the lowest cleaning efficiency of 36%. The membrane cleaning efficiency of the dead-end filtration unit (Fig. 11d) followed the same pattern as that of the cross-flow filtration unit but with some minor differences. The cleaning efficiency of the membrane cleaned with 1.5 M H_2O_2 was a bit lower than the one cleaned with 1.5 M NaClO. This may be attributed to the rate of reaction of the cleaning agents in relation to the extent of foulant deposition on both the surface and pores of each membrane. Generally, it has been reported that effective cleaning of foulants can be achieved with adequate duration whereas prolonged duration can possibly result in secondary fouling and even cause potential damage to the membrane when exposed to the high concentration of strong cleaning oxidants [27]. Based on this, it is envisaged that the cleaning efficiency of membranes cleaned with both NaClO and H_2O_2 may likely drop if their concentration is further increased.

4. Conclusion

This study has investigated the foulant composition and fouling formation mechanism of low-pressure PVDF-based membrane elements used in separating TiO_2 particles in the MBR system. This process was combined with one-time chemical cleaning, altogether accomplished via a simple but systematic approach. It was evident from the SEM-EDX and FTIR analysis that the elements S, Fe, O, Si, Ti and Al were the main constituents of the inorganic scales on the surface of the fouled membrane while FeS_2 and SiO_2 were the dominant inorganic compounds of the foulant. Meanwhile, the cleaned membranes revealed that these aforementioned foulants were almost completely removed by the one-time cleaning but H_2O_2 could not effectively remove O and Si. The obvious change in the crystalline characteristic peaks of the fouled membrane proves the dominance effect of the foulant on the surface of the membrane in the XRD diffractogram. The zeta potential of fouled, neat and cleaned membranes was predominantly negatively charged particular at higher pH which was explained by the electrostatic interaction existing between the foulant and the charge on the membrane surface. Drastic reduction in the contact angle of the fouled and cleaned membrane reveals the surface adhesion weakening caused by the foulant, thus resulting in a hydrophilic surface. The porosity, tortuosity and visual inspection results all show the impact of the foulant on the membrane elements. The permeation flux of the fouled membrane was significantly low compare to the neat membrane and the cleaning agents such as NaClO and H_2O_2 at selected concentrations were effective in flux recovery although, NaClO has a higher cleaning efficiency on a molar basis than H_2O_2. On the other hand, DI water as a cleaning agent could barely recover the flux of the fouled membrane.
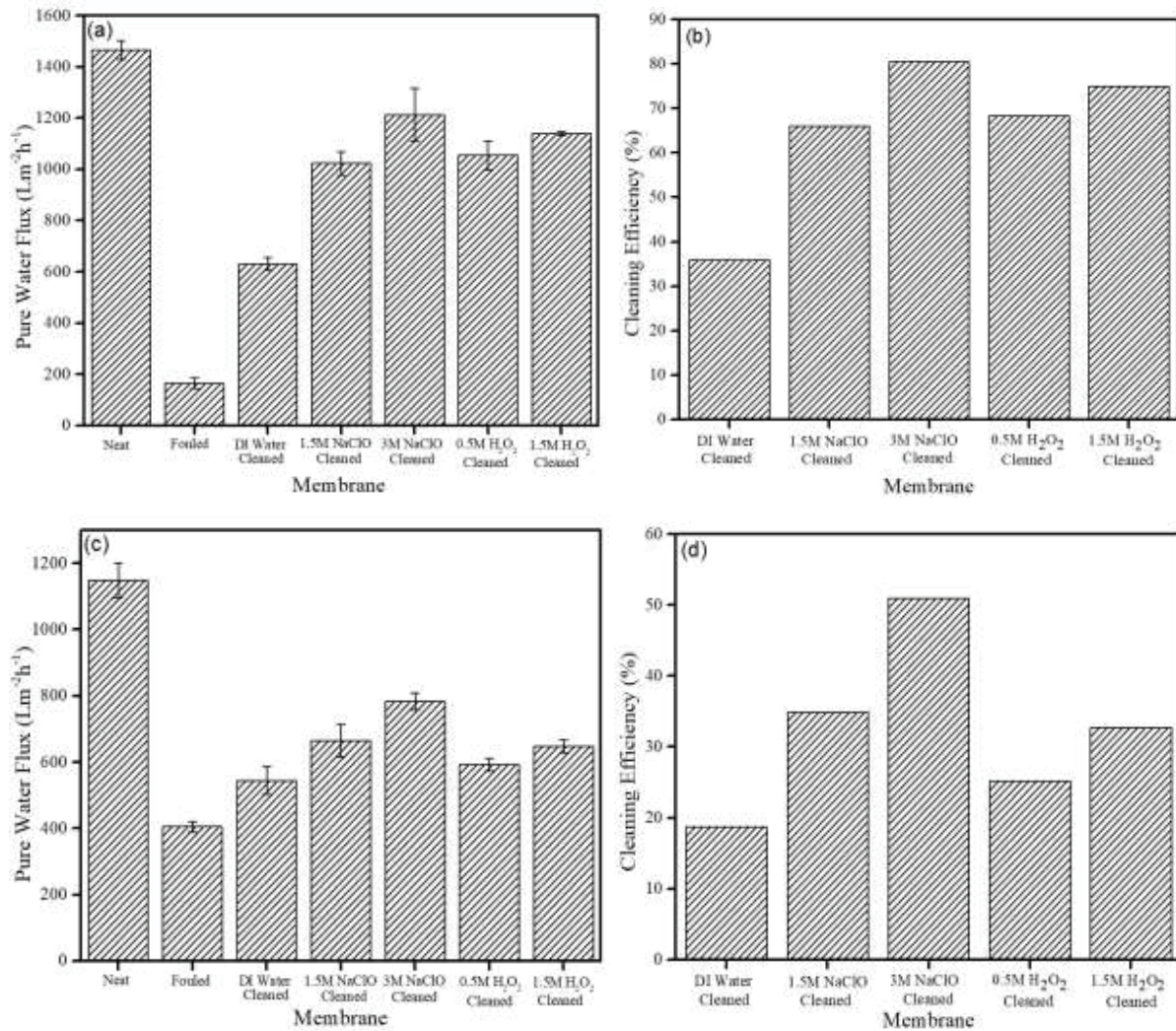
Fig. 11. Pure water flux and cleaning efficiency (or pure water flux recovery) of (a, b) cross-flow filtration unit and (c, d) dead-end filtration unit.

Acknowledgments

Declaration of interest

The authors declare no conflict of interest.

References

[1] W. Wu, X. Zhang, L. Qin, X. Li, Q. Meng, C. Shen, G. Zhang, Enhanced MPBR with polyvinylpyrrolidone-graphene oxide/PVDF hollow fiber membrane for efficient ammonia nitrogen wastewater treatment and high-density *Chlorella* cultivation, Chem. Eng. J., 379 (2020) 122368, doi: 10.1016/j.cej.2019.122368.

[2] R. Xu, W. Qin, B. Zhang, X. Wang, T. Li, Y. Zhang, X. Wen, Nanofiltration in pilot scale for wastewater reclamation: long-term performance and membrane biofouling characteristics, Chem. Eng. J., 395 (2020) 125087, doi: 10.1016/j.cej.2020.125087.

[3] B. Wang, K. Zhang, R.W. Field, Novel economical three-stage slug bubbling process in a large-scale flat-sheet membrane bioreactor of double deck configuration, AlChE J., 66 (2020) e16501, doi: 10.1002/aic.16501.

[4] B. Wang, K. Zhang, R.W. Field, Optimization of aeration variables in a commercial large-scale flat-sheet MBR operated with slug bubbling, J. Membr. Sci., 567 (2018) 181–190.

[5] Z. Zhang, M.W. Bligh, Y. Wang, G.L. Leslie, H. Bustamante, T.D. Waite, Cleaning strategies for iron-fouled membranes from submerged membrane bioreactor treatment of wastewaters, J. Membr. Sci., 475 (2015) 9–21.

[6] P. Buzatu, H. Qiblawey, A. Odai, J. Jamaleddin, M. Nasser, S.J. Judd, Clogging vs fouling in immersed membrane bioreactors, Water Res., 144 (2018) 46–54.

[7] Y. Chen, J. Teng, L. Shen, G. Yu, R. Li, Y. Xu, F. Wang, B. Liao, H. Lin, Novel insights into membrane fouling caused by gel layer in a membrane bioreactor: effects of hydrogen bonding, Bioresour. Technol., 276 (2019) 219–225.

[8] K. Zeng, J. Zhou, Z. Cui, Y. Zhou, C. Shi, X. Wang, L. Zhou, X. Ding, Z. Wang, E. Drioli, Insight into fouling behavior of poly (vinylidene fluoride) (PVDF) hollow fiber membranes caused by dextran with different pore size distributions, Chin. J. Chem. Eng., 26 (2018) 268–277.

[9] Y. Zen, Z. Mao, Y. Zhang, W. See, T. Haur, B. Wu, Enhancing fouling mitigation of submerged flat-sheet membranes by vibrating 3D-spacers, Sep. Purif. Technol., 215 (2019) 70–80.

[10] B. Ma, W. Xue, Y. Bai, R. Liu, W. Chen, H. Liu, Enhanced alleviation of ultrafiltration membrane fouling by regulating cake layer thickness with pre-coagulation during drinking water treatment, J. Membr. Sci., 596 (2020) 117732, doi: 10.1016/j.memsci.2019.117732.

[11] J. Teng, L. Shen, Y. He, B. Liao, G. Wu, H. Lin, Novel insights into membrane fouling in a membrane bioreactor: elucidating interfacial interactions with real membrane surface, Chemosphere, 210 (2018) 769–778.

[12] F. Liu, M.R.M. Abed, K. Li, Preparation and characterization of poly(vinylidene fluoride) (PVDF) based ultrafiltration membranes using nano γ-Al$_2$O$_3$, J. Membr. Sci., 366 (2011) 97–103.

[13] W. Lang, Z. Xuan, J. Shen, H. Xu, Z. Xu, Y. Guo, The contrastive study of chemical treatment on the properties of PVDF/PFSA and PVDF/PVP ultrafiltration membranes, Desalination, 341 (2014) 72–82.

[14] P. Bei, H. Liu, H. Yao, Y. Jiao, Y. Wang, L. Guo, Preparation and characterization of a PVDF membrane modified by an ionic liquid, Aust. J. Chem., 72 (2019) 425–433.

[15] W. Chen, Y. Liu, J. Liu, Selecting aeration in a PVDF flat-sheet membrane bioreactor for municipal wastewater treatment, Desal. Water Treat., 57 (2016) 6193–6201.

[16] G.D. Kang, Y.M. Cao, Application and modification of poly(vinylidene fluoride) (PVDF) membranes – a review, J. Membr. Sci., 463 (2014) 145–165.

[17] J. Suhartono, C. Tizaoui, Polyvinylidene fluoride membranes impregnated at optimised content of pristine and functionalised multi-walled carbon nanotubes for improved water permeation, solute rejection and mechanical properties, Sep. Purif. Technol., 154 (2015) 290–300.

[18] H.A.A. El-Rehim, E.A. Hegazy, D.A. Diaa, Photo-catalytic degradation of metanil yellow dye using TiO$_2$ immobilized into polyvinyl alcohol/acrylic acid microgels prepared by ionizing radiation, React. Funct. Polym., 72 (2012) 823–831.

[19] R. Thiruvenkatachari, T.O. Kwon, I.S. Moon, A total solution for simultaneous organic degradation and particle separation using photocatalytic oxidation and submerged microfiltration membrane hybrid process, Korean J. Chem. Eng., 22 (2005) 938–944.

[20] S. Lee, K. Choo, C. Lee, H. Lee, T. Hyeon, W. Choi, H. Kwon, Use of ultrafiltration membranes for the separation of TiO$_2$ photocatalysts in drinking water treatment, Ind. Eng. Chem. Res., 40 (2001) 1712–1719.

[21] S. Kagaya, K. Shimizu, R. Arai, K. Hasegawa, Separation of titanium dioxide photocatalyst in its aqueous suspensions by coagulation with basic aluminium chloride, Water Res., 33 (1999) 1753–1755.

[22] H.T. Wang, Y.Y. Ye, J. Qi, F.T. Li, Y.L. Tang, Removal of titanium dioxide nanoparticles by coagulation: effects of coagulants, typical ions, alkalinity and natural organic matters, Water Sci. Technol., 68 (2013) 1137–1143.

[23] A. Patchaiyappan, S. Saran, S.P. Devipriya, Recovery and reuse of TiO$_2$ photocatalyst from aqueous suspension using plant based coagulant – a green approach, Korean J. Chem. Eng., 33 (2016) 2107–2113.

[24] S. Mozia, Photocatalytic membrane reactors (PMRs) in water and wastewater treatment. A review, Sep. Purif. Technol., 73 (2010) 71–91.

[25] I.O. Uribe, A.M. Corral, J.L. Rodicio, S. Esplugas, Advanced technologies for water treatment and reuse, AlChE J. (Perspective), 61 (2015) 3146–3158.

[26] R. Damodar, S. You, G. Chiou, Investigation on the conditions mitigating membrane fouling caused by TiO$_2$ deposition in a membrane photocatalytic reactor (MPR) used for dye wastewater treatment, J. Hazard. Mater., 203–204 (2012) 348–356.

[27] E. Garmsiri, Y. Rasouli, M. Abbasi, A.A. Izadpanah, Chemical cleaning of mullite ceramic micro filtration membranes which are fouled during oily wastewater treatment, J. Water Process Eng., 19 (2017) 81–95.

[28] X. Shi, G. Tal, N.P. Hankins, V. Gitis, Fouling and cleaning of ultrafiltration membranes: a review, J. Water Process Eng., 1 (2014) 121–138.

[29] S. Hajibabania, A. Antony, G. Leslie, P.L. Clech, Relative impact of fouling and cleaning on PVDF membrane hydraulic performances, Sep. Purif. Technol., 90 (2012) 204–212.

[30] J. Saqib, I.H. Aljundi, Membrane fouling and modification using surface treatment and layer-by-layer assembly of polyelectrolytes: state-of-the-art review, J. Water Process Eng., 11 (2016) 68–87.

[31] Z. Wang, J. Ma, C.Y. Tang, K. Kimura, Q. Wang, Membrane cleaning in membrane bioreactors: a review, J. Membr. Sci., 468 (2014) 276–307.

[32] C. Regula, E. Carretier, Y. Wyart, G.G. Guiziou, A. Vincent, D. Boudot, P. Moulin, Chemical cleaning/disinfection and ageing of organic UF membranes: a review, Water Res., 6 (2014) 326–365.

[33] W. Ding, M. Chen, M. Zhou, Z. Zhong, Z. Cui, W. Xing, Fouling behavior of poly(vinylidene fluoride) (PVDF) ultrafiltration membrane by polyvinyl alcohol (PVA) and chemical cleaning method, Chin. J. Chem. Eng., 28 (2020) 3018–3026.

[34] V. Puspitasari, A. Granville, P.L. Clech, V. Chen, Cleaning and ageing effect of sodium hypochlorite on polyvinylidene fluoride (PVDF) membrane, Sep. Purif. Technol., 72 (2010) 301–308.

[35] K. Li, S. Li, T. Huang, C. Dong, J. Li, B. Zhao, S. Zhang, Chemical cleaning of ultrafiltration membrane fouled by humic substances: comparison between hydrogen peroxide and sodium hypochlorite, Int. J. Environ. Res. Public Health, 16 (2019) 2568, doi: 10.3390/ijerph16142568.

[36] K.H. Tng, A. Antony, Y. Wang, G.L. Leslie, Chapter 11 – Membrane Ageing During Water Treatment: Mechanisms, Monitoring, and Control, A. Basile, A. Cassano, N.K. Rastogi, Eds., Advances in Membrane Technologies for Water Treatment: Materials, Processes and Applications, Woodhead Publishing Series in Energy, Elsevier Ltd., Sawston Cambridge, United Kingdom, 2015, pp. 349–378.

[37] M.R.S. Sousa, J. Lora-García, M.-F. López-Pérez, M. Heran, Identification of foulants on polyethersulfone membranes used to remove colloids and dissolved matter from paper mill treated effluent, Water, 12 (2020) 365, doi: 10.3390/w12020365.

[38] P. Xu, C. Bellona, J.E. Drewes, Fouling of nanofiltration and reverse osmosis membranes during municipal wastewater reclamation: membrane autopsy results from pilot-scale investigations, J. Membr. Sci., 353 (2010) 111–121.

[39] A. Boubakri, S. Bouguecha, Diagnostic and membrane autopsy of Djerba Island desalination station, Desalination, 220 (2008) 403–411.

[40] B. Agnihotri, A. Sharma, A.B. Gupta, Characterization and analysis of inorganic foulants in RO membranes for groundwater treatment, Desalination, 491 (2020) 114567, doi: 10.1016/j.desal.2020.114567.

[41] A.S. Al-Amoudi, A.M. Farooque, Performance restoration and autopsy of NF membranes used in seawater pretreatment, Desalination, 178 (2005) 261–271.

[42] T. Tran, B. Bolto, S. Gray, M. Hoang, E. Ostarcevic, An autopsy study of a fouled reverse osmosis membrane element used in a brackish water treatment plant, Water Res., 41 (2007) 3915–3923.

[43] L. Zheng, D. Yu, G. Wang, Z. Yue, C. Zhang, Y. Wang, Characteristics and formation mechanism of membrane fouling in a full-scale RO wastewater reclamation process: membrane autopsy and fouling characterization, J. Membr. Sci., 563 (2018) 843–856.

[44] J. Jung, J. Ryu, S.Y. Choi, K.Y. Park, W.J. Song, Y.J. Yu, Y.-S. Jang, J. Park, J. Kweon, Autopsy study of irreversible foulants on polyvinylidene fluoride hollow-fiber membranes in an immersed microfiltration system operated for five years, Sep. Purif. Technol., 199 (2018) 1–8.

[45] M.T. Khan, Fouling of Seawater Reverse Osmosis (SWRO) Membrane: Chemical and Microbiological Characterization, Dissertation, King Abdullah University of Science & Technology (KAUST), Thuwal, Kingdom of Saudi Arabia, 2013.

[46] APHA, Standard Methods for the Examination of Water and Wastewater, American Public Health Association, America, 2012.

[47] L. Rezaei, M. Dehghani, A.H. Hassani, V. Alipour, Seawater reverse osmosis membrane fouling causes in a full scale desalination plant; through the analysis of environmental issues: raw water quality, Environ. Health Eng. Manage. J., 7 (2020) 119–126.

[48] K.H. Lasisi, W. Yao, T.F. Ajibade, H. Tian, F. Fang, K. Zhang, Impacts of sulfuric acid on the stability and separation performance of polymeric PVDF-based membranes at mild and high concentrations: an experimental study, Membranes, 10 (2020) 375, doi: 10.3390/membranes10120375.

[49] Q. Wang, H. Zeng, Z. Wu, J. Cao, Impact of sodium hypochlorite cleaning on the surface properties and performance of PVDF membranes, Appl. Surf. Sci., 428 (2018) 289–295.

[50] R. Golbandi, M.A. Abdi, A.A. Babaluo, A.B. Khoshfetrat, T. Mohammadlou, Fouling study of TiO_2 – boehmite MF membrane in defatting of whey solution: feed concentration and pH effects, J. Membr. Sci., 448 (2013) 135–142.

[51] A.S. Barnard, S.P. Russo, Shape and thermodynamic stability of pyrite FeS_2 nanocrystals and nanorods, J. Phys. Chem., 111 (2007) 11742–11746.

[52] A. Larsson, The size and shape of silica particles, Colloid. Polym. Sci., 277 (1999) 680–686.

[53] M.R. Bindhu, M. Umadevi, M.K. Micheal, M. Valan, N.A. Al-dhabi, Structural, morphological and optical properties of MgO nanoparticles for antibacterial applications, Mater. Lett., 166 (2016) 19–22.

[54] J.G. Dunn, W. Gong, D. Shi, A Fourier transform infrared study of the oxidation of pyrite, Thermochim. Acta, 208 (1992) 293–303.

[55] P. Vermelha, R.D. Janeiro, Processing and characterization of PET composites reinforced with geopolymer concrete waste, Mater. Res., 20 (2017) 411–420.

[56] H. Chang, T. Li, B. Liu, C. Chen, Q. He, J.C. Crittenden, Smart ultrafiltration membrane fouling control as desalination pretreatment of shale gas fracturing wastewater: the effects of backwash water, Environ. Int., 130 (2019) 104869, doi: 10.1016/j.envint.2019.05.063.

[57] M. Sun, I. Zucker, D.M. Davenport, X. Zhou, J. Qu, M. Elimelech, Reactive, self-cleaning ultrafiltration membrane functionalized with iron oxychloride nanocatalysts, Environ. Sci. Technol., 52 (2018) 8674–8683.

[58] I. Kovács, G. Veréb, S. Kertész, C. Hodúr, Z. László, Fouling mitigation and cleanability of TiO_2 photocatalyst-modified PVDF membranes during ultrafiltration of model oily wastewater with different salt contents, Environ. Sci. Pollut. Res., 25 (2018) 34912–34921.

[59] C. Wan, C.R. Bowen, Multiscale-structuring of polyvinylidene fluoride for energy harvesting: the impact of molecular-, micro- and macro-structure, J. Mater. Chem. A, 5 (2017) 3091–3128.

[60] M.F. Rabuni, N.M.N. Sulaiman, M.K. Aroua, N.A. Hashim, Effects of alkaline environments at mild conditions on the stability of PVDF membrane: an experimental study, Ind. Eng. Chem. Res., 52 (2013) 15874–15882.

[61] J. Meng, C. Chen, L. Huang, Q. Du, Y. Zhang, Surface modification of PVDF membrane via AGET ATRP directly from the membrane surface, Appl. Surf. Sci., 257 (2011) 6282–6290.

[62] C.H. Koo, A.W. Mohammad, F. Suja, Effect of cross-flow velocity on membrane filtration performance in relation to membrane properties, Desal. Water Treat., 55 (2014) 678–692.

[63] T. Xiao, P. Wang, X. Yang, X. Cai, J. Lu, Fabrication and characterization of novel asymmetric polyvinylidene fluoride (PVDF) membranes by the nonsolvent thermally induced phase separation (NTIPS) method for membrane distillation applications, J. Membr. Sci., 489 (2015) 160–174.

[64] Z. Arif, N.K. Sethy, L. Kumari, P.K. Mishra, B. Verma, Antifouling behaviour of $PVDF/TiO_2$ composite membrane: a quantitative and qualitative assessment, Iran. Polym. J. (English Ed.), 28 (2019) 301–312.

[65] Y.H. Teow, A.L. Ahmad, J.K. Lim, B.S. Ooi, Preparation and characterization of $PVDF/TiO_2$ mixed matrix membrane via in situ colloidal precipitation method, Desalination, 295 (2012) 61–69.

[66] L. Pisani, Simple expression for the tortuosity of porous media, Transp. Porous Media., 88 (2011) 193–203.

[67] M. Matyka, A. Khalili, Z. Koza, Tortuosity-porosity relation in porous media flow, P. Review E., 78 (2008) 1–8.

[68] H. Xie, T. Saito, M.A. Hickner, Zeta potential of ion-conductive membranes by streaming current measurements, Langmuir, 27 (2011) 4721–4727.

[69] J. Wang, S. Yang, W. Guo, H. Ngo, H. Jia, J. Yang, Characterization of fouling layers for in-line coagulation membrane fouling by apparent zeta, RSC Adv., 5 (2015) 106087–106093.

[70] Q. Wang, Z. Wang, Z. Wu, Effects of solvent compositions on physicochemical properties and anti-fouling ability of PVDF microfiltration membranes for wastewater treatment, Desalination, 297 (2012) 79–86.

[71] M.F. Rabuni, N.M.N. Sulaiman, N.A. Hashim, A systematic assessment method for the investigation of the PVDF membrane stability, Desal. Water Treat., 57 (2016) 1–12.

[72] E. Jigar, K. Bagi, Á. Fazekas, S. Kertész, G. Veréb, Filtration of BSA through TiO_2 photocatalyst modified PVDF membranes, Desal. Water Treat., 192 (2020) 392–399.

[73] X. Shen, Y. Zhao, X. Feng, S. Bi, W. Ding, L. Chen, Improved antifouling properties of PVDF membranes modified with oppositely charged copolymer, Biofouling: The Journal of Bioadhesion and Biofilm, 29 (2013) 331–343.

Supporting information

S1. Foulant chemical solubility analysis and foulant surface density tests

S1.1. Chemical solubility test

The chemical solubility test was carried out on the foulant which was gently scraped from the surface of the fouled membranes, in order to further understand its nature. Water, concentrated HCl and NaOH were used as the solubility solutions. Firstly, these solutions were prepared in three-round bottom conical flasks by (i) measuring 100 mL of DI water in one of the flasks and adding 0.1 g of the foulant into it (ii) preparing 5% concentrated HCl and adding 0.1 g of the foulant into it and (iii) dissolving 0.1 g of the foulant into 5% NaOH. After this, the round bottom conical flasks were vigorously shaken individually and left for about 2–5 min for further observation. The experiment set-up before and after the addition of foulant into the prepared solution is depicted in Fig. S1. The observation of the foulant dissolution in the solution is given in Table S1.

Fig. S1. Chemical solubility test experimental set-up (before and after the test).

Table S1
Summary outcome of the chemical solubility analysis

Solubility medium	Homogeneous solution	Colour change	Gas/heat evolution	Remark
Water	Insoluble	No change in color	No evolution occurred	No significant reaction was noticed
Acid	Soluble	Colour changes to light green	Evolution of heat occurred	Presence of Ti
Base	Partially soluble	Colour changes to reddish brown	No evolution occurred	Presence of Fe and S

S1.2. Foulant surface density

The degree/extent of the fouling on three fouled flat sheet membrane surface elements were determined in order to know their foulant surface density. This was achieved by measuring the mass of the foulant gotten from the surface of the membrane and dividing it by the surface area of the membrane. It was done upon membrane reception and after oven-drying the foulant at 105°C overnight. The average value with the standard deviation is given in Table S2.

Mathematically,

$$\text{FSD} \equiv \frac{\text{Mass of the foulant}(\text{kg})}{\text{Surface area of the membrane}(\text{m}^2)} \quad \text{(S1)}$$

Table S2
Calculation of the foulant surface density

Membrane	Mass of foulant (kg)	Membrane surface area (m^2)	FSD (kg m^{-2})	Mean FSD (kg m^{-2})
		Upon membrane reception		
Membrane 1	0.00406	0.12	0.034	
Membrane 2	0.00685	0.12	0.057	0.0045 ± 0.012
Membrane 3	0.00516	0.12	0.043	
		After oven-drying overnight at 105°C		
Membrane 1	0.00226	0.12	0.019	
Membrane 2	0.00312	0.12	0.026	0.0023 ± 0.002
Membrane 3	0.00278	0.12	0.023	

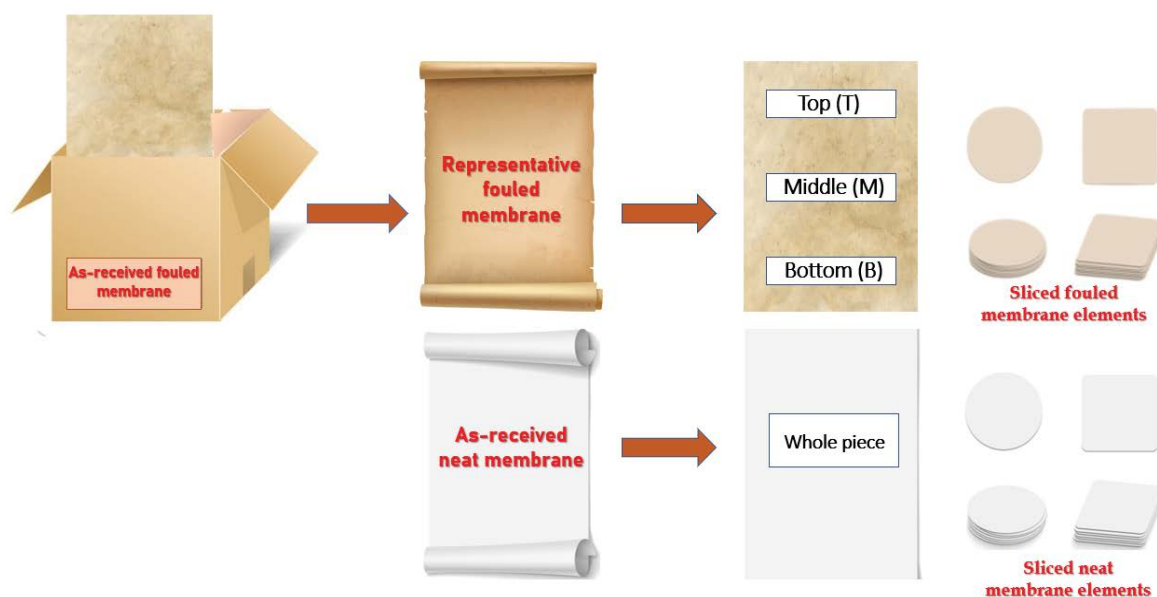## S2. Membrane sample preparation for characterization

Fig. S2. Schematic representation of the fouled and neat membrane elements preparation process for analysis.

S3. X-ray diffraction characteristic peaks

Table S3
Diffraction angles 2θ of their characteristic peaks

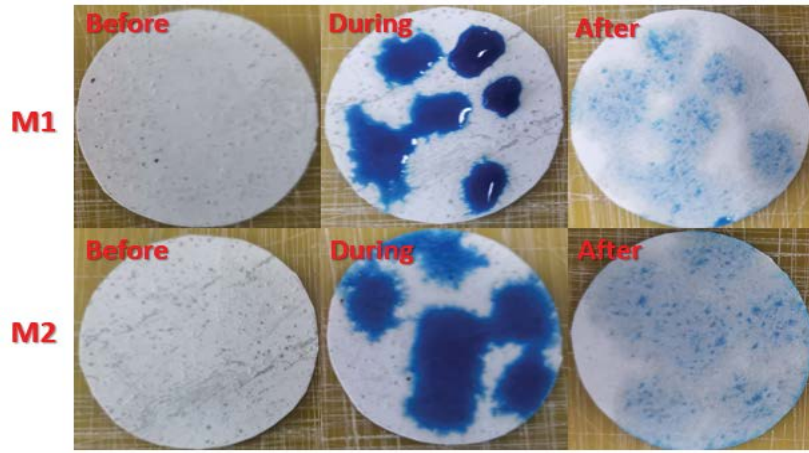| Cleaned membrane	Crystalline phase diffraction angles 2θ		
	α	β	α
DI water	17.80	20.82	25.99
NaClO @ 1.5 M	17.77	20.84	26.09
NaClO @ 3 M	17.74	20.92	26.04
H$_2$O$_2$ @ 0.5 M	17.82	20.84	26.12
H$_2$O$_2$ @ 1.5 M	17.80	20.95	26.02

S4. Dye test

Fig. S3. Dye methylene blue test result of the received fouled membranes surfaces.